Effects of side ratio on energy harvesting from transverse galloping of a rectangular cylinder

Haiyan Yu[1], Mingjie Zhang[2, *]

1. School of Civil Engineering, Dalian University of Technology, Dalian, 116024, China.

2. Department of Structural Engineering, Norwegian University of Science and Technology, Trondheim, 7491, Norway.

*Corresponding author: Mingjie Zhang, Email address: mingjie.zhang@ntnu.no

Abstract

Rectangular cylinders have been identified as ideal bluff bodies for galloping-based energy harvesting, while a systematic study of the effects of the side ratio (i.e., the ratio between the cylinder width and the cylinder height) remains unavailable. This study investigates the influences of the side ratio on the piezoelectric energy harvesting from the transverse galloping of a rectangular cylinder based on a representative electro-aero-mechanical model, in which the aerodynamic force is calculated by the quasi-steady theory. The existing experimental aerodynamic coefficients for rectangular cylinders with side ratios of 0.62 ~ 3.0 are utilized as inputs of the quasi-steady aerodynamic force model. The influences of the side ratio and load resistance on the onset velocity, displacement, and power output of the galloping-based energy harvester are investigated. The results show that the onset velocity of galloping is dependent on the load resistance while this dependency becomes less significant with increasing the natural frequency. The onset galloping velocity of the energy harvester decreases with increasing the side ratio, and the lowest onset velocity is achieved by a rectangular cylinder with a side ratio of around 2.50. The largest vibration amplitude is achieved by the cylinder with a side ratio of 1.62 or 2.0 at low flow velocities, while the largest vibration amplitude is always achieved by the square cylinder at high flow velocities. Therefore, the side ratio of a galloping-based energy harvester should be designed according to its working environment: the optimal side ratio is around 1.0 if the harvester is expected to work at relatively high reduced flow velocities, while the optimal side ratio is around 1.62 ~ 2.0 if the harvester is expected to be effective at relatively low reduced flow velocities. These conclusions can provide references for designing galloping-based energy harvesters with rectangular cylinders as bluff bodies.

Keywords: Piezoelectric energy harvesting; Galloping; Rectangular cylinder; Side ratio

1. Introduction

Slender flexible structures immersed in wind or water flows may be susceptible to various types of flow-induced vibrations including vortex-induced vibration, galloping, and flutter (in torsional or vertical-torsional coupled degrees of freedom). These dynamical instabilities have been observed in a great variety of engineering structures, e.g., long-span bridges [1, 2], cantilevered traffic sign supports [3], bridge cables [4], tall buildings and towers [5, 6], power transmission lines [7], and heat exchanger tube arrays [8], etc. Flow-induced vibrations are often undesirable in many structures since they may seriously impact the structural fatigue life and/or safety [2, 9]. On the other hand, energy harvesting from flow-induced vibrations has attracted increasing attention as a clean and sustainable energy source [10].

The mechanism for converting mechanical vibrations into electric power can be piezoelectric [11], electromagnetic [12], electrostatic [13], triboelectric [14], and their combinations [15]. Based on these converting mechanisms, energy harvesting can be achieved through vortex-induced vibrations (VIVs) [16, 17], galloping [18, 19], flutter [20], and their combinations [21-23]. Energy harvesting from the transverse galloping of a rectangular cylinder has been largely investigated due to the high performance related to the large vibration amplitude after an onset flow velocity for galloping instability. The investigation of transverse galloping was pioneered by Den Hartog [24], who proposed a criterion to determine the onset flow velocity based on the steady-state aerodynamic coefficients. Parkinson and co-authors [25-27] described the nonlinear galloping force with the quasi-steady theory and proposed to predict the vibration amplitude of transverse galloping based on the quasi-steady theory. They [27] further demonstrated that theory fails if galloping occurs at low reduced flow velocities and interferes with vortex-induced vibration. Hence, the applicability of the quasi-steady theory should be limited to structures with relatively large mass ratios (between structure and displaced fluid) and damping ratios. Following these pioneering studies, the transverse galloping of various structures has been extensively studied with special efforts paid to optimize the aerodynamic configurations and/or mitigate the undesired vibrations [28, 29].

The possibility of harvesting energy from transverse galloping was firstly proposed by Barrero-Gil et al. [30]. The authors [31, 32] also presented several theoretical investigations to optimize and enhance the performances of the galloping-based energy harvester based on a numerical system with the quasi-steady aerodynamic force model. Abdelkefi and co-authors [11, 33-35] attempted to study the performances of galloping-based energy harvesters through a series of theoretical and experimental investigations. They highlighted the roles of the bluff body configuration, the Reynolds number, the aerodynamic force representation, and the inclined angle on the performances of galloping-based energy harvesters. Yang et al.

[36] compared the performances of several galloping-based energy harvesters with different cross-sections through a series of wind tunnel experiments. Their results showed that the energy harvester with a square cylinder as the bluff body exhibits the best performance. Hémon et al. [37] and Andrianne et al. [38] studied the energy harvesting from flow-induced vibrations of rectangular cylinders based on the electromagnetic mechanism through wind tunnel experiments. He et al. [39] showed that a square cylinder performs interacted VIV and galloping, which is beneficial for the enhancement of wind energy harvesting. Zhang et al. [40] investigated the influences of the damping ratio and the mass ratio on the energy harnessing from flow-induced vibration of a square cylinder based on numerical simulations. Wang et al. [41] investigated the performance of an energy harvester with a hybrid bluff body composed of circular and square cross-sections through wind tunnel experiments and numerical simulations. Their results showed that the hybrid bluff body can couple the vibration characteristics of VIV and galloping, and hence remarkably reduce the onset flow velocity and increase the output voltage. Some aerodynamic modifications have also been introduced to enhance the energy harvesting from the flow-induced vibrations of rectangular cylinders [41, 42].

Although the performances of galloping-based energy harvesters with rectangular cylinders as bluff bodies have been investigated by several authors, the effects of the side ratio (i.e., the ratio between the cylinder width b and the cylinder height d) have rarely been studied. It is well-known that the flow regime around a rectangular cylinder and hence its galloping response is highly dependent on the side ratio b/d. Norberg [43] experimentally measured the steady-state aerodynamic coefficients of rectangular cylinders with various side ratios at a Reynolds number $Re = Ud/v = 13{,}000$, where U is the oncoming flow velocity and v is the kinematic viscosity. Their measurements suggest that the onset galloping velocity decreases with increasing the side ratio for $0.62 < b/d < 2.50$; however, a cylinder with $b/d = 3$ is always stable from galloping. Feero et al. [44] showed that the effect of side ratio on galloping instability is dependent on the Reynolds number. In the high Reynolds number range ($Re > 5000$), the observations of Norberg [43] were confirmed; however, in the low Reynolds number range ($Re < 2500$), rectangular cylinders with $b/d = 1$, 2, and 3 are all unstable from galloping and the onset velocity decreases with increasing the b/d. Zhang et al. [45] presented a numerical investigation on the effect of the side ratio ($b/d = 1/6 \sim 1.5$) on the energy harnessing from flow-induced vibration of rectangular cylinders. They analyzed an energy harvester with a low mass ratio $m^* = 1.725$, which exhibits interfered vortex-induced vibration and galloping [46]. They showed that the maximum power is achieved by a rectangular cylinder with $b/d = 1/6$. For an energy harvester with a large mass ratio (which exhibits typical galloping without interference between VIV), however, the effects of side ratio on the performance remain unknown.

This paper presents a numerical investigation to study the influences of the side ratio on the piezoelectric energy harvesting from the transverse galloping of a rectangular cylinder. A lumped-parameter model is employed to describe the coupled aero-electro-mechanical system of the galloping-based energy harvester, in which the quasi-steady theory is utilized to simulate the aerodynamic force. The experimental aerodynamic coefficients from Norberg [43] and Feero [44] are utilized as inputs of the quasi-steady aerodynamic force model. The performance of the galloping-based piezoelectric energy harvester is then evaluated for various side ratios. It is proved that the optimal side ratio for energy harvesting is around 1.0 if the harvester is expected to work at relatively high reduced flow velocities, while the optimal side ratio is around 1.62 ~ 2.0 if the harvester is expected to be effective at relatively low reduced flow velocities. The results of this paper should be limited to energy harvesters with relatively large mass ratios and high onset reduced velocities due to the limitation of the quasi-steady theory.

The subsequent parts of this paper are organized as follows. The lumped-parameter model for a galloping-based piezoelectric energy harvester is deduced and verified in Section 2. A linear analysis is presented in Section 3 to study the effects of the side ratio and the electrical load resistance on the onset galloping velocity of the coupled system. A nonlinear analysis of the coupled system is performed in Section 4 to investigate the effect of the side ratio on the displacement and power output of the galloping-based harvester. The main conclusions are summarized in Section 5.

2. Modeling of galloping-based piezoelectric energy harvester

The considered galloping-based piezoelectric energy harvester is schematically presented in figure 1. The energy harvester consists of a rectangular cylinder, a cantilever beam, and a piezoelectric transducer bonded at the root of the beam. The vibration of the beam can be excited by the aerodynamic force acting on the rectangular cylinder, which leads to power generation by the piezoelectric transducer. The lumped-parameter model for the aero-electro-mechanical system can be expressed as [11, 35]:

$$m[\ddot{y}(t) + 2\omega_0\xi_0\dot{y}(t) + \omega_0^2 y(t)] + \theta V(t) = F_y(t) \tag{1a}$$

$$\frac{V(t)}{R} + C_p\dot{V}(t) - \theta\dot{y}(t) = 0 \tag{1b}$$

where m represents the equivalent mass of the galloping-based piezoelectric energy harvester per unit length; y, $\dot{y}$, and $\ddot{y}$ denotes the transverse displacement, velocity, and acceleration of the rectangular cylinder, respectively; the overdot represents the derivative with respect to time t; ω_0 denotes the natural frequency in rad/s; ξ_0 is the mechanical damping ratio; F_y represents the aerodynamic force acting on the rectangular cylinder per unit length; V represents the generated voltage; C_p represents the capacitance of the piezoelectric

layer; R represents the electrical load resistance; θ is the electromechanical coupling coefficient.

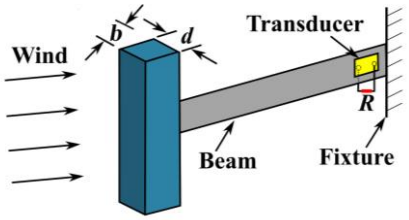

Figure 1. Schematic of a galloping-based energy harvester.

According to the quasi-steady theory, the aerodynamic force can be approximated as:

$$F_y = 0.5\rho U^2 d C_{Fy} = 0.5\rho U^2 d \sum_{i=1}^{N} A_i \left(\frac{\dot{y}}{U}\right)^i \tag{2}$$

where ρ is the fluid density; U is the oncoming flow velocity; d is the height of the cylinder; C_{Fy} represents the aerodynamic lift force coefficient; A_i ($i = 1 \sim N$) are aerodynamic damping coefficients obtained through the polynomial fitting based on the experimental $C_{Fy}(\alpha)$ curve; α is the angle of attack, i.e., the angle between the oncoming flow direction and the chord line of the rectangular cylinder. For a rectangular cylinder symmetric about the chord line, only odd-order terms are necessary for the polynomial expansion since even-order terms contribute insignificantly to the overall dynamics [2, 47].

It is worth noting that the applicability of the quasi-steady theory should be limited to cases at relatively high reduced flow velocities $U_r = U/\omega_0 d$, where the time scale for the incident flow to pass through the cylinder and arrive sufficiently far downstream is considerably lower than that of the cylinder vibration [2]. The experiments of Washizu et al. [48] and Ma et al. [49] showed that the quasi-steady theory can simulate the aerodynamic forces on a vibrating square cylinder very well for $2\pi U_r > 10$. As a result, the quasi-steady theory is capable of accurately simulating the galloping of a cylinder with relatively large mass-damping parameters (i.e., Scruton number, $Sc = 4\pi m\xi_0/\rho d^2$), while its accuracy decreases with decreasing the Scruton number.

By substituting equation (2) into equation (1) and introducing the dimensionless variables $\tau = \omega_0 t$, $Y = y/d$, and $I = \theta V/m\omega_0^2 d$, equation (1) can be expressed in the dimensionless form as:

$$Y'' + 2\xi_0 Y' + Y + I = \frac{U_r^2}{2m^*} \sum_{i=1}^{N} A_i \left(\frac{Y'}{U_r}\right)^i \tag{3a}$$

$$I + C_p R\omega_0 I' = 2\xi_E Y' \tag{3b}$$

where the prime represents the derivative with respect to the dimensionless time τ; $m^* = m/\rho d^2$ is the mass ratio between the harvester and the displaced fluid; $\xi_E = \theta^2 R/2m\omega_0$ is a dimensionless damping coefficient due to the coupling of the dynamics of the rectangular cylinder and the piezoelectric generator.

The aerodynamic coefficient C_{Fy} for a square cylinder (i.e., a rectangular cylinder with $b/d = 1$) is presented

in figure 2 as a function of the angle of attack α. The results of Smith [50], Norberg [43], and Feero et al. [44] were measured in smooth flows at Re = 22,300, 13,000, and 10,000, respectively. It is noted that the aerodynamic coefficients measured by different authors agree very well, indicating that the C_{Fy} is almost independent of Re in the considered Re range. However, it should be clarified that C_{Fy} may be remarkably affected by the oncoming flow intensity and other experimental conditions (e.g., the blocking ratio and end conditions).

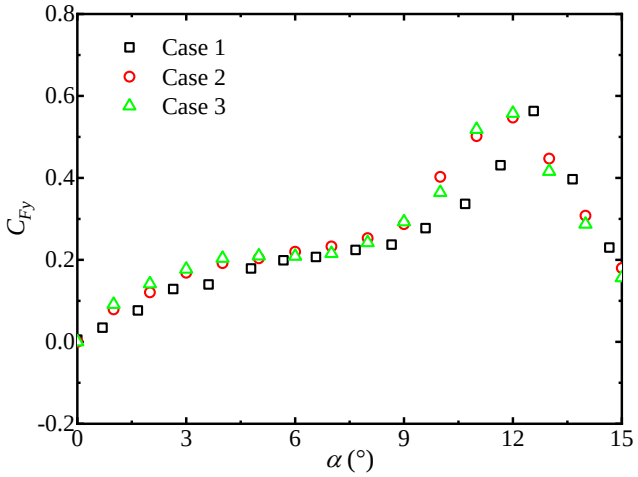

Figure 2. Experimental aerodynamic coefficients of a square cylinder versus angle of attack (Case 1 from [50], Re = 22,300; Case 2 from [43], Re = 13,000; Case 3 from [44], Re = 10,000).

To demonstrate the predictive capability of the quasi-steady theory, the galloping responses of a square cylinder are predicted at several mass-damping conditions using the aerodynamic coefficients of Smith [50] and Norberg [43], respectively. The coefficients of Smith [50] are fitted as a 9th-order polynomial following [26], i.e., A_1 = 2.69, A_3 = −168, A_3 = 6,270, A_3 = −59,900. The coefficients of Norberg [43] are fitted as a 17th-order polynomial with A_i listed in table 1. The fitted aerodynamic coefficients versus angle of attack will be presented later. In the following analysis, A_i listed in table 1 will be utilized to calculate the aerodynamic forces acting on the rectangular cylinder of the energy harvester as shown in figure 1. The predictions are compared with available experimental measurements [26, 51] in figure 3, in which the reduced flow velocity U_r and the dimensionless amplitude A_Y are multiplied by $\pi A_1/Sc$. The theoretical predictions at various mass-damping conditions collapse to a single curve in this manner [52]. It is noted that there is a hysteresis phenomenon in the variation of the vibration amplitude versus the flow velocity, which has been analyzed in detail by several authors [47, 53]. The theoretical predictions by two groups of aerodynamic coefficients agree very well with discrepancies noticeable only at low reduced flow velocities. The results for Sc = 15.6 ~ 53.2 agree well with the theoretical predictions, while the accuracy of the predictions decreases for Sc = 9.6 and 12.1. For Sc = 3.7, the theoretical predictions deviate significantly from the experimental measurements. Accordingly, the quasi-

steady theory is capable of accurately simulating the galloping of a square cylinder with $Sc > 10$.

Table 1. Polynomial representations of the aerodynamics coefficients

Cylinder	A_1	A_3	A_5	A_7	A_9	A_{11}	A_{13}	A_{15}	A_{17}
$b/d = 1.0$ [43]	4.68	−3.99e2	1.19e4	3.85e5	−2.61e7	5.34e8	−5.28e9	2.58e10	−5.00e10
$b/d = 1.62$ [43]	4.82	−2.81e2	3.71e4	−2.40e6	7.21e7	−1.17e9	1.06e10	−5.05e10	9.90e10
$b/d = 2.50$ [43]	13.0	−2.56e3	2.09e5	−9.50e6	2.51e8	−3.94e9	3.63e10	−1.81e11	3.76e11
$b/d = 1.0$ [44]	5.60	−1.00e3	1.21e5	−8.03e6	2.96e8	−5.80e9	5.33e10	−1.27e11	−6.41e11
$b/d = 2.0$ [44]	8.46	3.50e2	1.66e5	−3.26e7	2.09e9	−6.66e10	1.15e12	−1.03e13	3.74e13

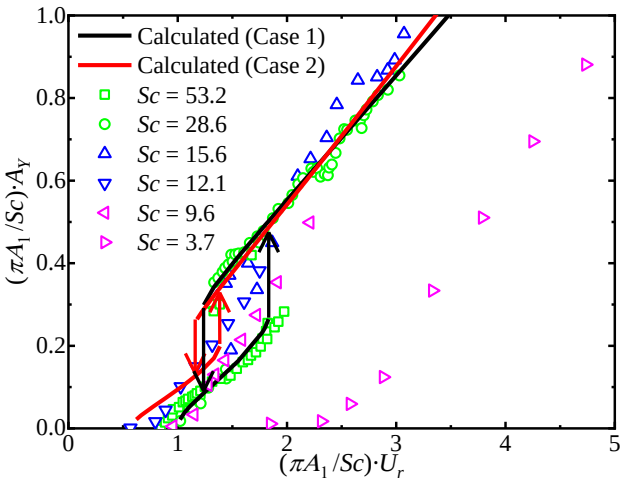

Figure 3. Comparison of experimental vibration amplitudes and predicted results by quasi-steady theory. Data of $Sc = 53.2$, 28.6, 15.6 originate from [26] and data of $Sc = 12.1$, 9.6, 3.7 originate from [51].

To validate the numerical model for the galloping-based piezoelectric energy harvester given in equation (1), the voltage outputs are calculated for the case tested by Yang et al. [54]. Figure 4 compares the experimentally obtained and numerically simulated voltage outputs. The aerodynamic coefficients utilize the values of Laneville [55] (measured in a turbulent flow with intensity around 6.7% and $Re = 33{,}000$) because the experiment of Yang et al. [54] is conducted in a turbulent flow. It can be seen that the numerical simulations agree satisfactorily with the experimental results. The deviations can be ascribed to the errors of the piezoelectric modeling, the errors of the aerodynamic coefficients, the impact of the aerodynamic force representation, and the different flow conditions of the experiments of Laneville [55] and Yang et al. [54], etc. Considering these possible errors, it is believed that the lumped-parameter model can be used to simulate the behavior of the galloping-based piezoelectric energy harvester with reasonable accuracy. Hence, the representative electro-aero-mechanical model of equation (1) can be utilized to study the effects of side ratio on the performances of galloping-based piezoelectric energy harvesters.

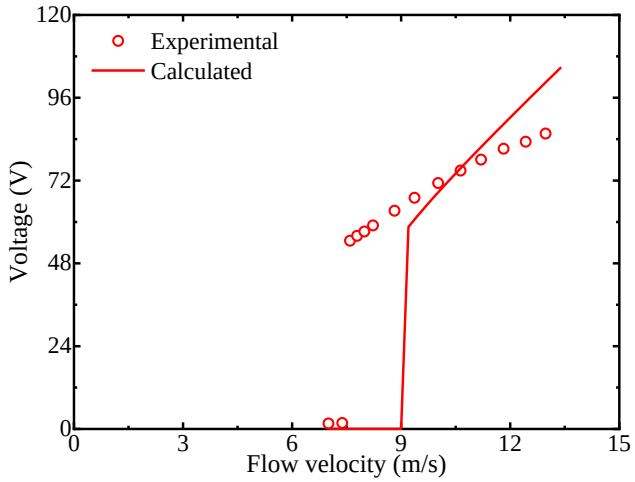

Figure 4. Comparison of experimental voltages [54] and predicted results.

In the following analysis, the mechanical and electrical parameters are m = 0.44 kg/m, ξ_0 = 0.13%, d = 0.015 m, θ = 1.55 mN/V, and C_p = 1.55 mN/V, as considered by Abdelkefi et al. [11]. The effect of the side ratio will be investigated for energy harvesters with different electrical load resistances and natural frequencies.

3. Linear analysis: Effects of side ratio on onset galloping velocity

The effects of the side ratio and the electrical load resistance on the onset galloping velocity are determined from a linear analysis of the coupled aero-electro-mechanical system. It is known that the onset galloping velocity is $U_r = 4m^*\xi_0/A_1$ for a pure aeroelastic system without the piezoelectric coupling effect [2, 47]. On the other hand, the onset galloping velocity for a coupled aero-electro-mechanical system can be determined through a complex eigenvalue analysis of the equations of motion. Introducing the following state variables:

$$\mathbf{X} = \begin{bmatrix} X_1 \\ X_2 \\ X_3 \end{bmatrix} = \begin{bmatrix} Y \\ Y' \\ I \end{bmatrix} \tag{4}$$

The dimensionless equations of motion, i.e., equation (3), can be linearized as:

$$X_1' = X_2 \tag{5a}$$

$$X_2' = -X_1 - (2\xi_0 - \frac{U_r}{2m^*}A_1)X_2 - X_3 \tag{5b}$$

$$X_3' = \frac{2\xi_E X_2}{C_p R\omega_0} - \frac{X_3}{C_p R\omega_0} \tag{5c}$$

Equation (5) can be expressed in a matrix form as:

$$\mathbf{X}' = \mathbf{G}\mathbf{X} \tag{6a}$$

$$\mathbf{G} = \begin{bmatrix} 0 & 1 & 0 \\ -1 & -(2\xi_0 - \frac{U_r}{2m^*}A_1) & -1 \\ 0 & \frac{2\xi_E}{C_p R\omega_0} & -\frac{1}{C_p R\omega_0} \end{bmatrix} \tag{6b}$$

The matrix **G** consists of all parameters that influence the linear stability of the aero-electro-mechanical

system. Hence, this matrix can be utilized to study the effects of the side ratio and the electrical load resistance on the onset velocity of galloping.

The three eigenvalues (λ_j, $j = 1 \sim 3$) of the aero-electro-mechanical system can be obtained through a complex eigenvalue analysis of the matrix **G**. The first two eigenvalues are similar to those of the traditional galloping system without the electromechanical coupling effect. The third eigenvalue, which is always real and negative, is due to the electromechanical coupling effect. The first two eigenvalues are a pair of complex conjugates, i.e., $\lambda_1 = \lambda_2^*$. The real part of the conjugate pair reflects the damping and the absolute value of their imaginary part represents the damped vibration frequency of the coupled system. The stability of the linearized system is determined by the real part of the first two eigenvalues: the system is asymptotically stable if the real part is negative while it is unstable if the real part is positive. The onset galloping velocity is achieved when the real part of the first two eigenvalues becomes zero.

The experimentally obtained A_1 values in [43, 44, 46, 51, 56] are shown in figure 5 as a function of side ratio b/d. These results were all measured in a Reynolds number range higher than 10,000, in which the flow regime and hence the A_1 value is expected to be relatively insensitive to the Reynolds number [44]. The results of Blevins [56] and Mannini et al. [46] are collected from several previous studies. The data reviewed by Mannini et al. [46] are given as short lines since the data are scattered in a considerable range. It is noted that the A_1 values of various authors are slightly different, which might be a result of the differences between various experiments, e.g., the boundary conditions, the blocking ratios, and the surface roughnesses, as well as the uncertainty in calculating the derivative from experimental data. Despite the difference between various experimental data, their global trends consistently suggest that A_1 increases and hence the onset galloping velocity decreases with increasing the side ratio for $b/d < 2.5$. The A_1 value exhibits a sharp change and the cylinder becomes stable from galloping at a critical side ratio within $2.5 < b/d < 3.0$.

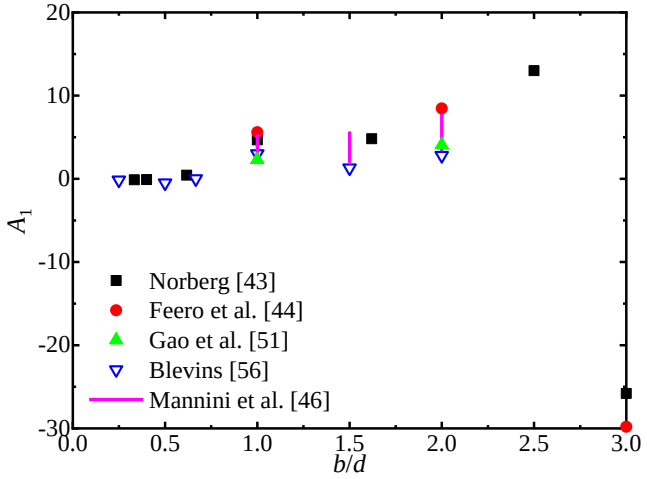

Figure 5. Variation of galloping criterion A_1 versus side ratio b/d.

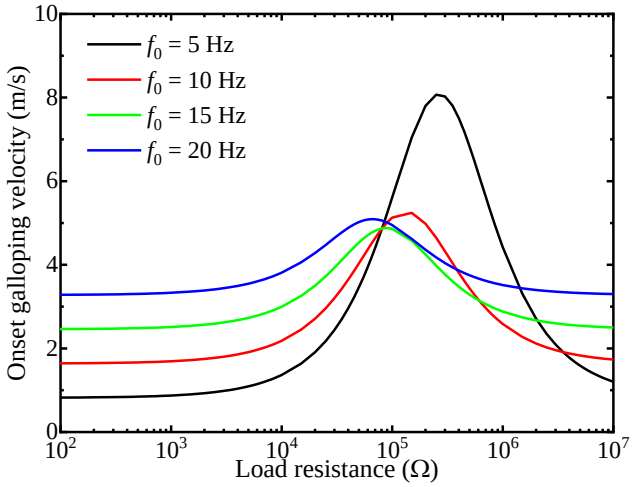

Figure 6. Variation of onset galloping velocity versus electrical load resistance for energy harvester with square cylinder

Figure 6 shows the variation of onset galloping velocity versus electrical load resistance for the energy harvester with a square cylinder calculated by the aerodynamic coefficient of Norberg [43]. Four natural frequencies are considered, i.e., $f_0 = \omega_0/2\pi$ = 5, 10, 15, and 20 Hz, respectively. For an aero-electro-mechanical system with very low electrical load resistance, the damping introduced by the piezoelectric coupling effect is insignificant and hence the onset velocity should be close to that for a pure aeroelastic system.

It is noticed from figure 6 that, for each natural frequency, the onset galloping velocity varies remarkably with the load resistance. In the range of lower load resistances, the variation of onset flow velocity is small. The variation rate increases with increasing the load resistance and the onset velocity achieves a peak value within $R = 5\times10^4 \sim 5\times10^5$. The load resistance corresponding to the highest onset velocity is dependent on the natural frequency of the energy harvester. For higher load resistances, the onset velocity reduces and finally reaches a value close to that for a system with very low resistance. It is interesting to note that the onset velocity becomes less sensitive to the load resistance with increasing the natural frequency. This is because the damping ratio introduced by the piezoelectric coupling effect ($\xi_E = \theta^2 R/2m\omega_0$ in equation (3)) reduces as $f_0 = \omega_0/2\pi$ becomes larger. It is important to note that the damping due to the piezoelectric coupling cannot be fully represented by ξ_E, especially for a case with $C_p R\omega_0$ close to or larger than one [31]. However, the overall damping effect is inversely proportional to $f_0 = \omega_0/2\pi$.

Figure 7 presents the variation of the onset galloping velocity versus the electrical load resistance for energy harvesters with rectangular cylinders of b/d = 0.62, 1.0, 1.62, 2.0, and 2.50. The results are calculated based on the A_1 values of Norberg [43] or Feero et al. [44], as presented in figure 5. The rectangular cylinders of b/d = 0.25 and 3.0 are stable from galloping and hence the results are not presented in figure 7. The natural frequency is considered as f_0 =10 Hz. It is noted that the onset galloping velocity generally decreases with

increasing b/d in the considered range of side ratio. The onset galloping velocity for the cylinder of b/d = 0.60 is much higher than those for other cylinders, and the results at around $R = 10^4 \sim 10^6$ are not included in this figure due to the extremely high onset velocities. For the cylinder of b/d = 1.0, two groups of results are available, while these two groups are slightly different due to the different A_1 values of Norberg [43] or Feero et al. [44]. The onset galloping velocity for b/d = 1.62 is very close to that for b/d = 1.0. Due to the experimental differences, the onset velocity for b/d = 1.62 (calculated by the A_1 value of Norberg [43]) lies between the two groups of results for b/d = 1.0 calculated by the A_1 values of [43] and [44]. Finally, the onset velocity for the cylinder of b/d = 2.50 is considerably lower than those of other cylinders. The linear analysis suggests that the onset galloping velocity of the energy harvester can be decreased by increasing the side ratio, and the lowest onset velocity is achieved by a rectangular cylinder with a side ratio of around 2.50.

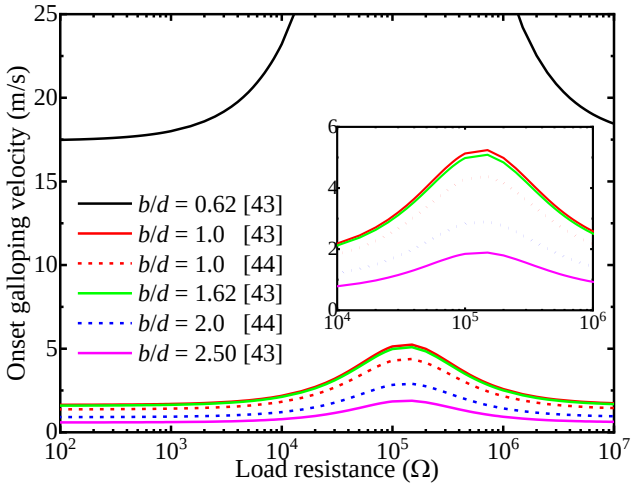

Figure 7. Variation of onset galloping velocity versus electrical load resistance for energy harvesters with rectangular cylinders of various side ratios

4. Nonlinear analysis

A nonlinear analysis of the coupled aero-electro-mechanical system is performed in this section to investigate the effect of the side ratio on the displacement and power output of the galloping-based energy harvester. The aerodynamic coefficients adopt the experimental results of Norberg [43] or Feero et al. [44], as presented in figure 8. The experimental coefficients are fitted as 17th-order polynomials with A_i listed in table 1. Energy harvesters with rectangular cylinders of b/d = 1.0, 1.62, 2.0, and 2.5 are considered, while the cylinder of b/d = 0.62 is not considered because it is ineffective due to the very high onset galloping velocity. Two groups of aerodynamic coefficients are available for the cylinder of b/d = 1.0, and hence the results for this side ratio are calculated based on each group of aerodynamic coefficients. The mechanical and electrical parameters are the same as those utilized in Section 3 and the natural frequency is considered as f_0 =10 Hz. The coupled equations of motion are solved numerically by using the Newmark-β method. The simulations

were performed by increasing the oncoming flow velocity over the range of 0 to 15 m/s with an incremental of 0.2 m/s. At the flow velocity of 0 m/s, the initial dimensionless displacement is set as 0.01 and the initial dimensionless velocity and voltage are both zero. The initial displacement at any other flow velocity is set equal to the stable displacement of the formerly analyzed velocity to simulate the continuously increasing flow velocity. The normalized time step of the simulations is $\Delta\tau = 1/100$, and the simulation for each flow velocity is performed sufficiently long to obtain the steady response of the coupled system.

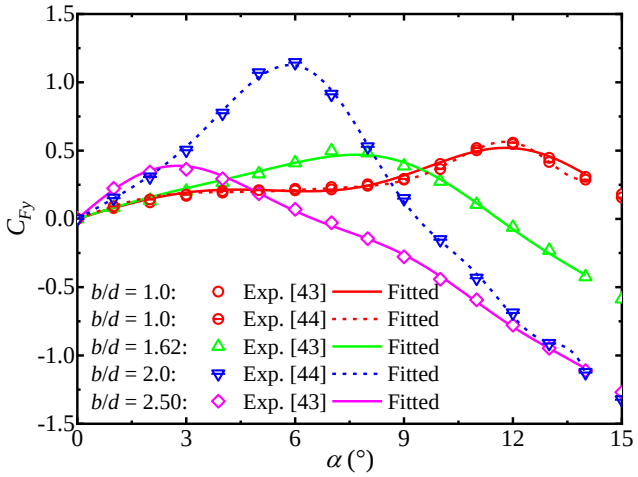

Figure 8. Experimental and fitted aerodynamic coefficients of rectangular cylinders of various side ratios (Data from [43], *Re* = 13,000; Data from [44], *Re* = 10,000).

The effects of the electrical load resistance on the transverse displacement and the power output of the coupled system are firstly investigated. Figures 9(a, c, e) shows the variations of the dimensionless transverse displacements versus the load resistance for energy harvesters with rectangular cylinders of various side ratios. Three flow velocities are considered, i.e., U = 4, 8, and 14 m/s. It follows from figure 9(a, c, e) that the transverse displacements first decrease and then increase with increasing the load resistance for all side ratios. The displacements reach the minimum values when the load resistance is around $R = 10^5$ Ω. This can be explained by the maximum value of the electromechanical damping in this range of electrical load resistances. The transverse displacements for some cases in figure 9(a) are zero since the onset galloping velocities of these cases are higher than 4 m/s. At U = 4 m/s, the largest vibration amplitude is achieved by the cylinder of b/d = 1.62 or 2.0. However, at U = 8 m/s, the largest vibration amplitude is achieved by the cylinder of b/d = 1.0, 1.62, or 2.0 depending on the load resistance. Finally, at U = 8 and 14 m/s, the largest vibration amplitude is always achieved by the cylinder with b/d = 1.0.

Figures 9(b, d, f) shows the variations of the power outputs versus the load resistance for energy harvesters with rectangular cylinders of various side ratios. It is noted that the power outputs for b/d = 2.0 and 2.5 first increase with increasing the load resistance and reach the maximum values around $R = 10^5$ Ω, after which the

power outputs start to decrease. The ranges of load resistances over which the harvested power is higher are consistent with the ranges of load resistances over which transverse displacement reaches the minimum. For b/d = 1.0 and 1.62 at low flow velocities (e.g., U = 4 m/s), there exist two optimal values of the load resistances at which the power outputs reach peak values, while the power outputs are very low between the two optimal load resistances. This is induced by the sharp jumps of the vibration amplitude, as shown by the red and green lines in figure 9(a). The sharp jumps of the vibration amplitude will be explained later. At U = 4 and 8 m/s, the largest power output is achieved by the cylinder of b/d = 2.0 around $R = 10^5$ Ω. However, at U = 14 m/s, the largest power output is achieved by the cylinder of b/d = 1.0 at the same load resistance.

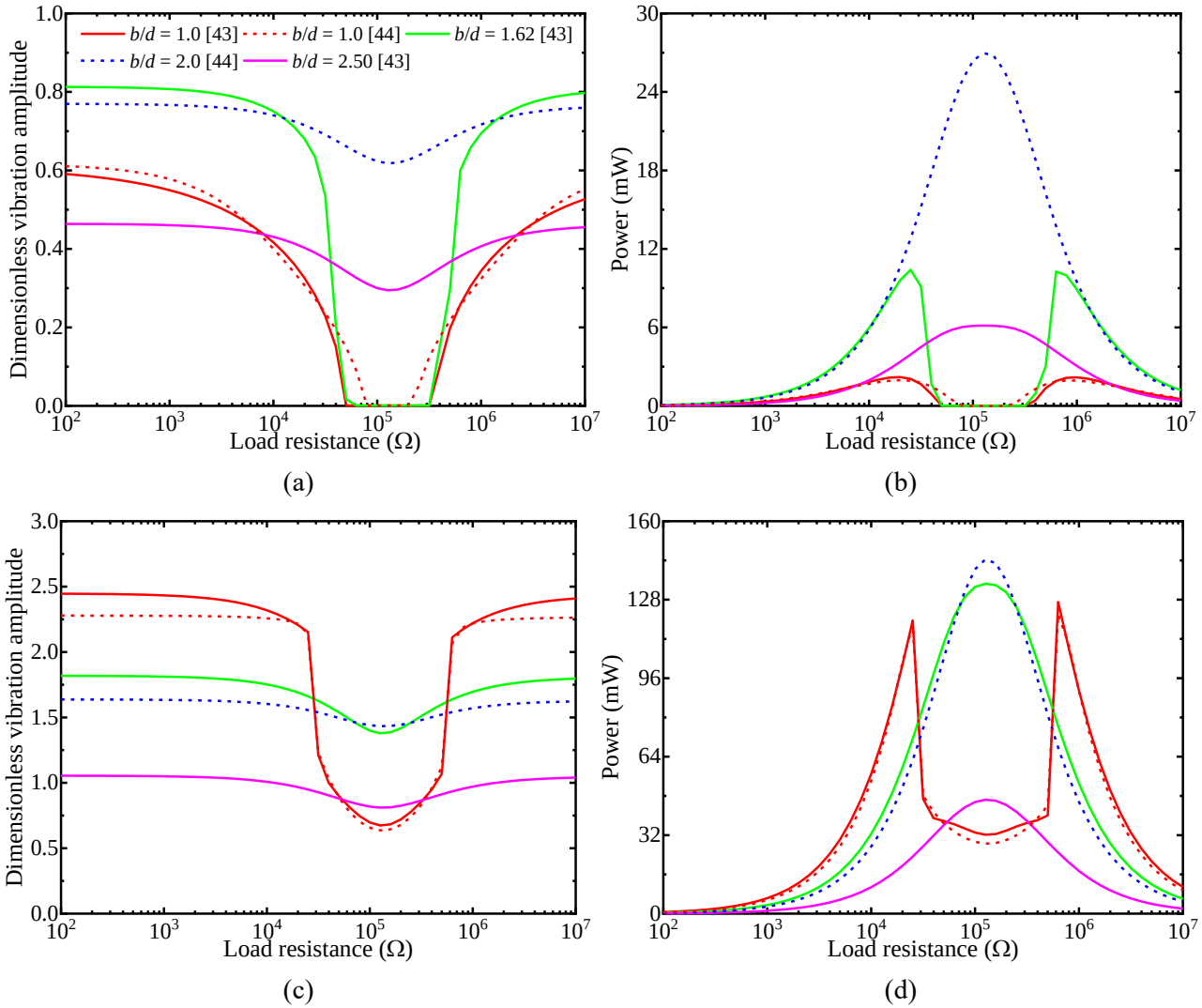

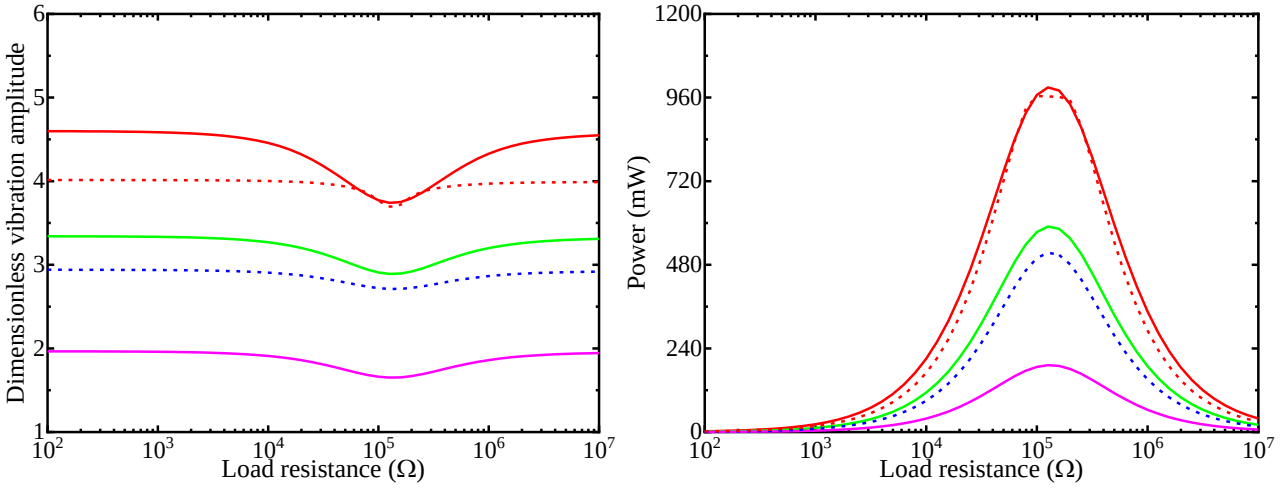

Figure 9. Variation of transverse displacement and power output versus electrical load resistance for energy harvesters with rectangular cylinders of various side ratios: (a) and (b) $U = 4$ m/s, (c) and (d) $U = 8$ m/s, (e) and (f) $U = 14$ m/s.

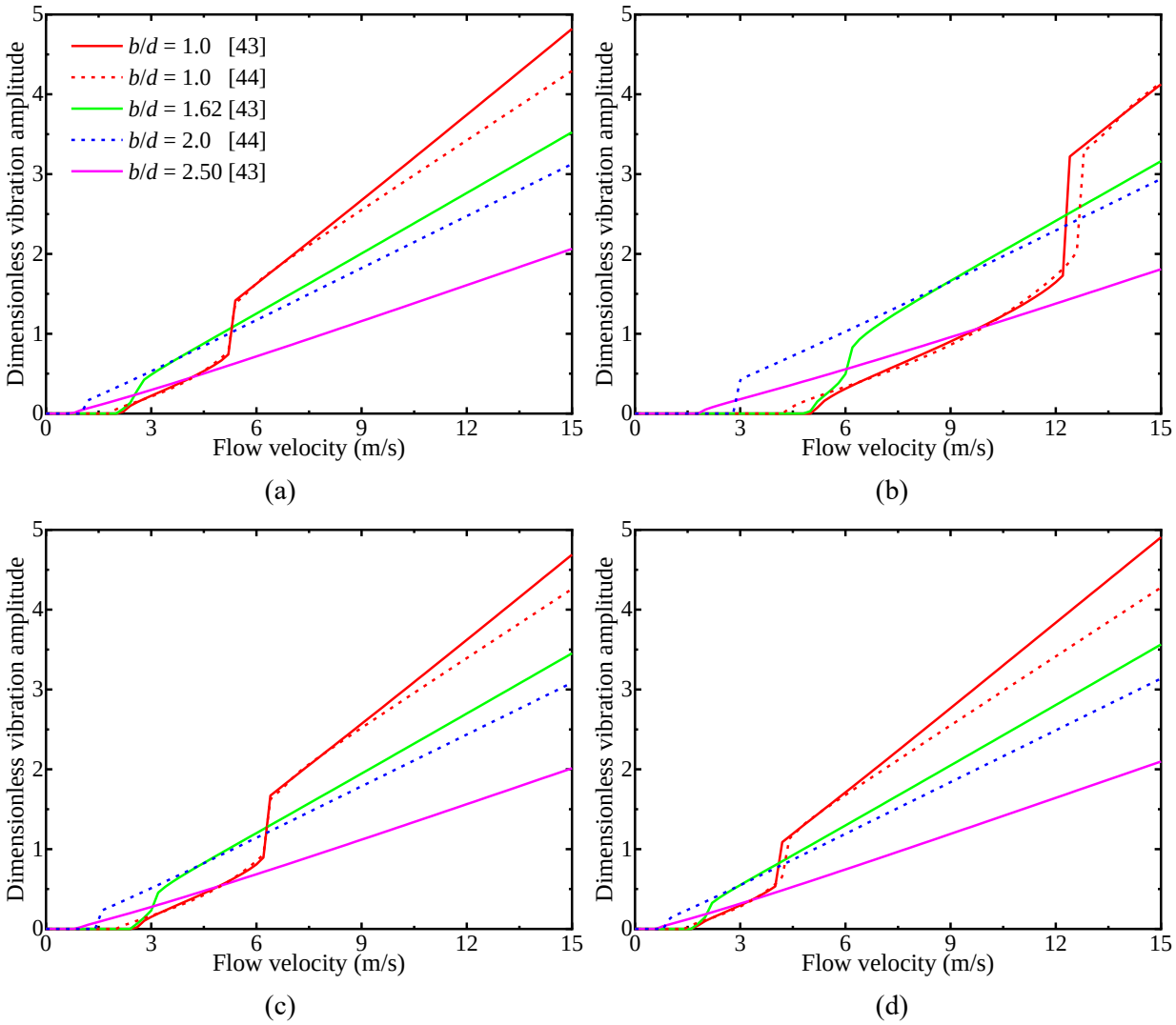

Figure 10. Bifurcation diagrams for transverse displacements of energy harvesters with rectangular cylinders of various side ratios: (a) $R = 10^4$ Ω, (b) $R = 10^5$ Ω, (c) $R = 10^6$ Ω, and (d) $R = 10^7$ Ω.

Figure 10 presents the effects of the side ratio and the load resistance on the transverse displacements of

the energy harvesters with rectangular cylinders of various side ratios. The results are given for four load resistances, i.e., $R = 10^4$, 10^5, 10^6, and 10^7 Ω, respectively. It is noted that both the onset velocity and the slope of the bifurcation curve are affected by the side ratio. At low flow velocities, the cylinder of $b/d = 1.62$ or 2.0 exhibits the largest transverse displacements. At high flow velocities, the largest transverse displacements are always achieved by the cylinder of $b/d = 1.0$. Although the onset velocities for rectangular cylinders of $b/d = 1.0$ and 1.62 are very close, the cylinders exhibit significantly different galloping responses. It is also interesting to note that the transverse displacements are lower in the middle range of load resistance values of $R = 10^5$ Ω, which is consistent with the observations in figure 9(a, c, e). The vibration amplitude for a cylinder of $b/d = 1.0$ or 1.62 exhibits a sharp jump, which occurs due to the hysteresis phenomenon in the variation of the vibration amplitude versus the flow velocity. If the simulations were performed by decreasing the oncoming flow velocity, the jump of the vibration amplitude would occur at a lower flow velocity. At $U = 4$ and 8 m/s, the vibration belongs to the branches before or after the sharp jump depending on the load resistance. Hence, there are sharp jumps in the variation of the vibration amplitude versus the load resistance, as shown in figure 9(a, c). At $U = 14$ m/s, the vibrations always belong to the branch after the sharp jump, and hence the vibration amplitude varies continuously with the load resistance, as shown in figure 9(e).

Figures 11 show the variations of power outputs versus flow velocity for the energy harvesters with rectangular cylinders of various side ratios. At low flow velocities, the cylinder of $b/d = 1.62$ or 2.0 exhibits the largest transverse displacements. At high flow velocities, the largest transverse displacements are always achieved by the cylinder of $b/d = 1.0$. Therefore, the optimal side ratio of a galloping-based energy harvester with a rectangular cylinder is dependent on its working flow velocities. The optimal side ratio is around 1.0 if the energy harvester is expected to work at relatively high reduced flow velocities, while the optimal side ratio is around 1.62 ~ 2.0 if the energy harvester is expected to start at relatively low reduced flow velocities.

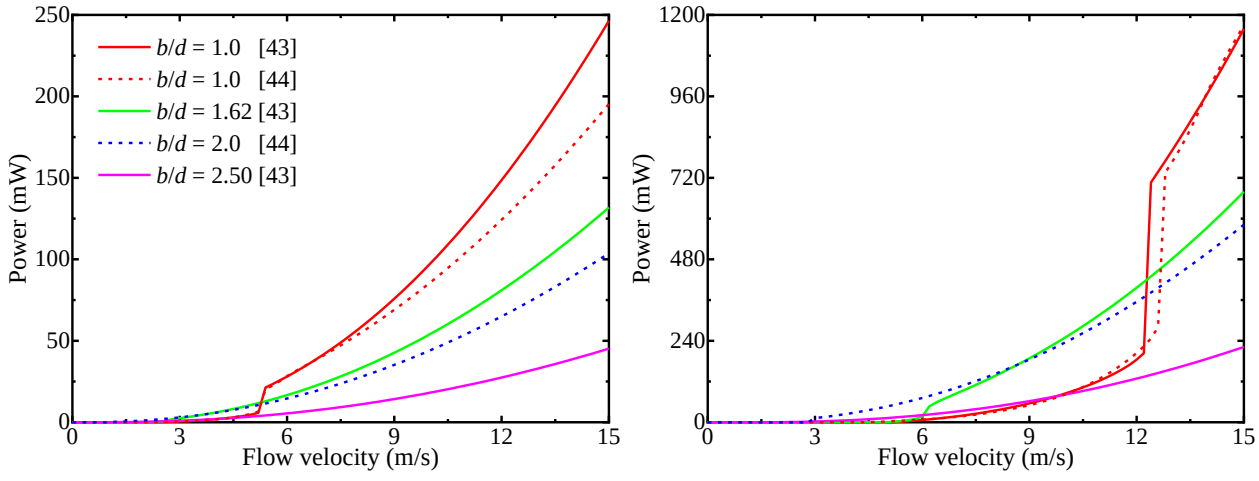

(a) (b)

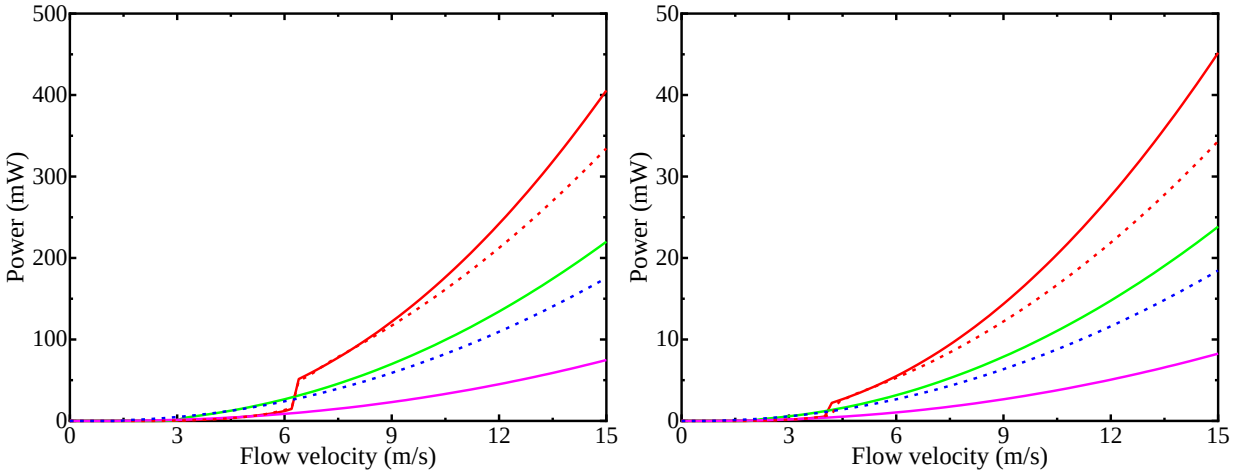

Figure 11. Bifurcation diagrams for power outputs of energy harvesters with rectangular cylinders of various side ratios: (a) $R = 10^4$ Ω, (b) $R = 10^5$ Ω, (c) $R = 10^6$ Ω, and (d) $R = 10^7$ Ω.

5. Conclusions

This paper presents a numerical investigation to study the influences of the width-to-height side ratio b/d on the piezoelectric energy harvesting from the transverse galloping of a rectangular cylinder. The galloping-based energy harvester is simulated as a lumped-parameter model, in which the quasi-steady theory is utilized to calculate the aerodynamic force. Rectangular cylinders of b/d = 0.62, 1.0, 1.62, 2.0, and 2.50 are considered. Rectangular cylinders with side ratios out of the considered range are ineffective since they have very high onset galloping velocities or they are stable from galloping. Due to the limitation of the quasi-steady theory, the results of this paper should be limited to energy harvesters with relatively large mass ratios (between structure and displaced fluid) and high onset reduced velocities.

A linear analysis is presented to study the effects of the side ratio and the load resistance on the onset galloping velocity of the coupled system. The results show that the onset velocity of galloping is dependent on the load resistance while the dependency becomes less significant with increasing the natural frequency of the energy harvester. The onset galloping velocity of the energy harvester can be decreased by increasing the side ratio, and the lowest onset velocity is achieved by a rectangular cylinder with a side ratio of around 2.50.

A nonlinear analysis of the coupled system is performed to investigate the effect of the side ratio on the displacement and power output of the galloping-based energy harvester. At low flow velocities, the largest vibration amplitude is achieved by the cylinder of b/d = 1.62 or 2.0, and the optimal side ratio for energy harvesting lies within or around this range. However, at higher flow velocities, the largest vibration amplitude is always achieved by the cylinder with b/d = 1.0, and the maximum harvested power is achieved by this side ratio. In conclusion, the optimal side ratio for energy harvesting is around 1.0 if the harvester is expected to work at relatively high reduced flow velocities, while the optimal side ratio is around 1.62 ~ 2.0 if the harvester

is expected to be effective at relatively low reduced flow velocities. These conclusions can help in the designing of a galloping-based energy harvester with a rectangular cylinder as the bluff body.

Declaration of competing interest

The authors declare that they have no known competing financial interests or personal relationships that could have appeared to influence the work reported in this paper.

References

1. Zhang, M., Xu, F., Ying, X., *Experimental investigations on the nonlinear torsional flutter of a bridge deck.* Journal of Bridge Engineering, 2017. **22**(8): p. 04017048.
2. Zhang, M., Xu, F., Han, Y., *Assessment of wind-induced nonlinear post-critical performance of bridge decks.* Journal of Wind Engineering and Industrial Aerodynamics, 2020. **203**: p. 104251.
3. Johns, K.W., Dexter, R.J., *The development of fatigue design load ranges for cantilevered sign and signal support structures.* Journal of Wind Engineering and Industrial Aerodynamics, 1998. **77**: p. 315-326.
4. Xu, F., Yu, H., Zhang, M., Han, Y., *Experimental study on aerodynamic characteristics of a large-diameter ice-accreted cylinder without icicles.* Journal of Wind Engineering and Industrial Aerodynamics. **208**: p. 104453.
5. Kawai, H., *Effects of angle of attack on vortex induced vibration and galloping of tall buildings in smooth and turbulent boundary layer flows.* Journal of wind engineering and industrial aerodynamics, 1995. **54**: p. 125-132.
6. Zhang, M., Xu, F., Øiseth, O., *Aerodynamic damping models for vortex-induced vibration of a rectangular 4: 1 cylinder: Comparison of modeling schemes.* Journal of Wind Engineering and Industrial Aerodynamics, 2020. **205**: p. 104321.
7. Song, Y., Liu, Z., Rønnquist, A., Nåvik, P., Liu, Z., *Contact wire irregularity stochastics and effect on high-speed railway pantograph–catenary interactions.* IEEE Transactions on Instrumentation and Measurement, 2020. **69**(10): p. 8196-8206.
8. Paı, M., *Real-life experiences with flow-induced vibration.* Journal of fluids and structures, 2006. **22**(6-7): p. 741-755.
9. Song, Y., Wang, Z., Liu, Z., Wang, R., *A spatial coupling model to study dynamic performance of pantograph-catenary with vehicle-track excitation.* Mechanical Systems and Signal Processing, 2021. **151**: p. 107336.
10. Wang, J., Geng, L., Ding, L., Zhu, H., Yurchenko, D., *The state-of-the-art review on energy harvesting from flow-induced vibrations.* Applied Energy, 2020. **267**: p. 114902.
11. Abdelkefi, A., Hajj, M., Nayfeh, A., *Piezoelectric energy harvesting from transverse galloping of bluff bodies.* Smart Materials and Structures, 2012. **22**(1): p. 015014.
12. Chen, Z., Xia, Y., He, J., Xiong, Y., Wang, G., *Elastic-electro-mechanical modeling and analysis of piezoelectric metamaterial plate with a self-powered synchronized charge extraction circuit for vibration energy harvesting.* Mechanical Systems and Signal Processing, 2020. **143**: p. 106824.
13. Lai, Z., Wang, J., Zhang, C., Zhang, G., Yurchenko, D., *Harvest wind energy from a vibro-impact DEG embedded into a bluff body.* Energy Conversion and Management, 2019. **199**: p. 111993.
14. Tao, K., Yi, H., Yang, Y., Chang, H., Wu, J., Tang, L., Yang, Z., Wang, N., Hu, L., Fu, Y., *Origami-inspired electret-based triboelectric generator for biomechanical and ocean wave energy harvesting.* Nano Energy, 2020. **67**: p. 104197.
15. Lai, Z., Wang, S., Zhu, L., Zhang, G., Wang, J., Yang, K., Yurchenko, D., *A hybrid piezo-dielectric wind energy harvester for high-performance vortex-induced vibration energy harvesting.* Mechanical Systems and Signal Processing. **150**: p. 107212.
16. Qin, W., Deng, W., Pan, J., Zhou, Z., Du, W., Zhu, P., *Harvesting wind energy with bi-stable snap-through excited by vortex-induced vibration and galloping.* Energy, 2019. **189**: p. 116237.

17. Wang, J., Zhou, S., Zhang, Z., Yurchenko, D., *High-performance piezoelectric wind energy harvester with Y-shaped attachments.* Energy conversion and management, 2019. **181**: p. 645-652.
18. Zhu, H., Gao, Y., *Hydrokinetic energy harvesting from flow-induced vibration of a circular cylinder with two symmetrical fin-shaped strips.* Energy, 2018. **165**: p. 1259-1281.
19. Wang, J., Tang, L., Zhao, L., Zhang, Z., *Efficiency investigation on energy harvesting from airflows in HVAC system based on galloping of isosceles triangle sectioned bluff bodies.* Energy, 2019. **172**: p. 1066-1078.
20. Bryant, M., Garcia, E., *Modeling and testing of a novel aeroelastic flutter energy harvester.* Journal of vibration and acoustics, 2011. **133**(1).
21. Sun, H., Ma, C., Bernitsas, M.M., *Hydrokinetic power conversion using Flow Induced Vibrations with cubic restoring force.* Energy, 2018. **153**: p. 490-508.
22. Sun, H., Ma, C., Bernitsas, M.M., *Hydrokinetic power conversion using Flow Induced Vibrations with nonlinear (adaptive piecewise-linear) springs.* Energy, 2018. **143**: p. 1085-1106.
23. Ding, L., Zhang, L., Wu, C., Mao, X., Jiang, D., *Flow induced motion and energy harvesting of bluff bodies with different cross sections.* Energy Conversion and Management, 2015. **91**: p. 416-426.
24. Den Hartog, J.P., *Mechanical vibrations*. 1985: Courier Corporation.
25. Parkinson, G., Brooks, N., *On the aeroelastic instability of bluff cylinders.* 1961.
26. Parkinson, G., Smith, J., *The square prism as an aeroelastic non-linear oscillator.* The Quarterly Journal of Mechanics and Applied Mathematics, 1964. **17**(2): p. 225-239.
27. Parkinson, G., Wawzonek, M., *Some considerations of combined effects of galloping and vortex resonance.* Journal of Wind Engineering and Industrial Aerodynamics, 1981. **8**(1-2): p. 135-143.
28. Tamura, T., Miyagi, T., *The effect of turbulence on aerodynamic forces on a square cylinder with various corner shapes.* Journal of Wind Engineering and Industrial Aerodynamics, 1999. **83**(1-3): p. 135-145.
29. Dai, H., Abdelkefi, A., Wang, L., *Usefulness of passive non-linear energy sinks in controlling galloping vibrations.* International Journal of Non-Linear Mechanics, 2016. **81**: p. 83-94.
30. Barrero-Gil, A., Alonso, G., Sanz-Andres, A., *Energy harvesting from transverse galloping.* Journal of Sound and Vibration, 2010. **329**(14): p. 2873-2883.
31. Vicente-Ludlam, D., Barrero-Gil, A., Velazquez, A., *Optimal electromagnetic energy extraction from transverse galloping.* Journal of Fluids and Structures, 2014. **51**: p. 281-291.
32. Vicente-Ludlam, D., Barrero-Gil, A., Velazquez, A., *Enhanced mechanical energy extraction from transverse galloping using a dual mass system.* Journal of Sound and Vibration, 2015. **339**: p. 290-303.
33. Abdelkefi, A., Yan, Z., Hajj, M.R., *Modeling and nonlinear analysis of piezoelectric energy harvesting from transverse galloping.* Smart materials and Structures, 2013. **22**(2): p. 025016.
34. Abdelkefi, A., Yan, Z., Hajj, M.R., *Performance analysis of galloping-based piezoaeroelastic energy harvesters with different cross-section geometries.* Journal of Intelligent Material Systems and Structures, 2014. **25**(2): p. 246-256.
35. Javed, U., Abdelkefi, A., *Impacts of the aerodynamic force representation on the stability and performance of a galloping-based energy harvester.* Journal of Sound and Vibration, 2017. **400**: p. 213-226.
36. Yang, Y., Zhao, L., Tang, L., *Comparative study of tip cross-sections for efficient galloping energy harvesting.* Applied Physics Letters, 2013. **102**(6): p. 064105.
37. Hémon, P., Amandolese, X., Andrianne, T., *Energy harvesting from galloping of prisms: A wind tunnel experiment.* Journal of Fluids and Structures, 2017. **70**: p. 390-402.
38. Andrianne, T., Aryoputro, R.P., Laurent, P., Colson, G., Amandolese, X., Hémon, P., *Energy harvesting from different aeroelastic instabilities of a square cylinder.* Journal of Wind Engineering and Industrial Aerodynamics, 2018. **172**: p. 164-169.
39. He, X., Yang, X., Jiang, S., *Enhancement of wind energy harvesting by interaction between vortex-induced vibration and galloping.* Applied Physics Letters, 2018. **112**(3): p. 033901.

40. Zhang, B., Mao, Z., Song, B., Ding, W., Tian, W., *Numerical investigation on effect of damping-ratio and mass-ratio on energy harnessing of a square cylinder in FIM.* Energy, 2018. **144**: p. 218-231.
41. Wang, J., Gu, S., Zhang, C., Hu, G., Chen, G., Yang, K., Li, H., Lai, Y., Litak, G., Yurchenko, D., *Hybrid wind energy scavenging by coupling vortex-induced vibrations and galloping.* Energy Conversion and Management, 2020. **213**: p. 112835.
42. Sun, W., Jo, S., Seok, J., *Development of the optimal bluff body for wind energy harvesting using the synergetic effect of coupled vortex induced vibration and galloping phenomena.* International Journal of Mechanical Sciences, 2019. **156**: p. 435-445.
43. Norberg, C., *Flow around rectangular cylinders: pressure forces and wake frequencies.* Journal of wind engineering and industrial aerodynamics, 1993. **49**(1-3): p. 187-196.
44. Feero, M.A., Naguib, A.M., Koochesfahani, M.M., *Influence of geometry on the galloping instability of rectangular cylinders in the Reynolds number range 1,000–10,000.* Journal of Fluids and Structures, 2020. **94**: p. 102881.
45. Zhang, B., Wang, K.-H., Song, B., Mao, Z., Tian, W., *Numerical investigation on the effect of the cross-sectional aspect ratio of a rectangular cylinder in FIM on hydrokinetic energy conversion.* Energy, 2018. **165**: p. 949-964.
46. Mannini, C., Marra, A., Bartoli, G., *VIV–galloping instability of rectangular cylinders: Review and new experiments.* Journal of wind engineering and industrial aerodynamics, 2014. **132**: p. 109-124.
47. Barrero-Gil, A., Sanz-Andrés, A., Alonso, G., *Hysteresis in transverse galloping: the role of the inflection points.* Journal of Fluids and Structures, 2009. **25**(6): p. 1007-1020.
48. Washizu, K., Ohya, A., Otsuki, Y., Fujii, K., *Aeroelastic instability of rectangular cylinders in a heaving mode.* Journal of Sound and Vibration, 1978. **59**(2): p. 195-210.
49. Ma, C., Liu, Y., Li, Q., Liao, H., *Prediction and explanation of the aeroelastic behavior of a square-section cylinder via forced vibration.* Journal of Wind Engineering and Industrial Aerodynamics, 2018. **176**: p. 78-86.
50. Smith, J.D., *An experimental study of the aeroelastic instability of rectangular cylinders*. 1962, University of British Columbia.
51. Gao, G., Zhu, L., Li, J., Han, W., *Modelling nonlinear aerodynamic damping during transverse aerodynamic instabilities for slender rectangular prisms with typical side ratios.* Journal of Wind Engineering and Industrial Aerodynamics, 2020. **197**: p. 104064.
52. Novak, M., *Galloping oscillations of prismatic structures.* Journal of Engineering Mechanics, 1972.
53. Luo, S., Chew, Y., Ng, Y., *Hysteresis phenomenon in the galloping oscillation of a square cylinder.* Journal of Fluids and Structures, 2003. **18**(1): p. 103-118.
54. Yang, X., He, X., Li, J., Jiang, S., *Modeling and verification of piezoelectric wind energy harvesters enhanced by interaction between vortex-induced vibration and galloping.* Smart Materials and Structures, 2019. **28**(11): p. 115027.
55. Laneville, A., *Effects of turbulence on wind induced vibrations of bluff cylinders*. 1973, University of British Columbia.
56. Blevins, R.D., *Flow-induced vibration.* vnr, 1977.